2022년 8월
석사학위논문

A protocol for recovery of a rat tibia fracture through 3D scaffold implantation

조선대학교 대학원

의 과 학 과

김 대 옥

A protocol for recovery of a rat tibia fracture through 3D scaffold implantation

백서 경골 골절 회복을 위한 3D 스캐폴드 이식 프로토콜

2022년 8월 26일

조선대학교 대학원

의 과 학 과

김 대 옥

A protocol for recovery of a rat tibia fracture through 3D scaffold implantation

지도교수 임 원 봉

이 논문을 공학 석사학위신청 논문으로 제출함

2022년 4월

조선대학교 대학원

의 과 학 과

김 대 옥

김대옥의 석사학위논문을 인준함

위원장	조선대학교	교　수	손 홍 문 (인)
위　원	조선대학교	교　수	김 동 휘 (인)
위　원	조선대학교	부교수	임 원 봉 (인)

2022년　5월

조선대학교 대학원

CONTENTS

LIST OF FIGURES

ABSTRACT

백서 경골 골절 회복을 위한 3D 스캐폴드 이식 프로토콜

김 대 옥
지도교수 : 임 원 봉
조선대학교 대학원 의과학과

서론: 최근 골절을 치유하는 방법 중 하나는 환자 맞춤형 3D 프린팅을 적용하는 것으로, 골절부의 결손 부위를 맞춤형으로 제작한 임플란트를 정확히 출력해 이식하는 것이 최적 골절 치유 방법이다.

이 연구에서는 표준화된 3D 프린팅 프로세스 구현을 위해, 골절 모델을 만들고 그 맞춤형 3D 프린팅을 제작하며 이식할 수 있는 전체 프로세스를 진행하여 동물 실험을 통해 적용해 보고자 하였다.

실험 및 방법: 골절치료 3D 프린팅 프로세스를 정립하고 골절모델을 제작하여, X-ray와 micro-CT 이미지를 획득하고, 이미지 전처리 소프트웨어를 사용해 분할과 재구성을 하여 골절된 뼈를 추출하였다. 이를 바탕으로 골절부위 스캐폴드를 3차원 모델링하고 3D프린팅으로 출력하여 골절부위에 이식한 후, 방사선 검사를 통해 3D 프린팅 프로토콜을 실험으로 확인하고자 하였다.

결과: 골절 모델을 만들고 그 맞춤형 3D 프린팅 골편을 제작하여 결함 부위에 이식할 수 있는 전체 프로세스를 3D 프린팅으로 적용하는 과정을 수행하였다.

논의: 3D 프린팅 프로토콜 진행에 따른 골절 회복 프로세스에 대한 동물 임상 검증과 조직학적 연구의 필요성이 있다.

결론: X-ray와 micro-CT 영상을 활용해 비정형적 골절을 맞춤형으로 대체하는 3D프린팅 스캐폴드의 식립 과정을 수행하여, 골절 치료에 새로운 역할을 할 것으로 기대된다.

색인단어: 경골, 골절, 3D 프린팅, 스캐폴드, 골형성, 맞춤형

Ⅰ. INTRODUCTION

Fractures are considered a major health challenge associated with an aging population worldwide, and the need for fracture healing research is expanding. As we enter the age of global aging, insufficient surgical and pharmacological treatment due to osteoporotic musculoskeletal weakness and increased personal treatment cost has led the increase in fracture disease. In particular, hip fractures occurring in the elderly are recognized as serious fractures with high prevalence and mortality. In 2050, more than 50% of fractures in the world are expected to occur in Asia, and as osteoporotic fractures accompany them, it may increase the burden of social medical expenses in the future.[1)]

The traditional method of treating fractures is to perform reduction to bring the broken bone back to its normal position. Reduction proceeds with a closed reduction of fractures without surgery by returning a bone or bone fragment to its original position through manual techniques. In severe cases with multiple bone fragments, open reduction internal fixation (ORIF) surgery is performed using prostheses such as pins, screws, rods, and plates. These include open reduction, plate fixation, external fixation, intramedullary fixation, internal fixation, and minimally invasive plate fixation using an external plate. After reduction is performed, an X-ray is usually taken to confirm that the fractured bone is in its normal position. After a closed reduction of the fracture, most fractures are fixed with a cast or splint until the fracture is healed. However, since long-term immobilization causes joint stiffness and muscle contraction, prompt rehabilitation exercise is recommended immediately after fracture healing.[2)]

Another bone grafting method is to insert properly cut autologous bone, allograft bone, xenograft bone, and synthetic bone for the missing interosseous space. In autogenous bone grafting, bone fragments from other parts of the body, such as the pelvis, are cut and used. This procedure is ideal and can be performed immediately even when the space between the bone fragments is too large, and can be performed later in the case of delay or non-union. However, there is a limit to the amount and shape of the grafted bone, and the morbidity of the donor site may increase during the extraction process or after collection. Xenogeneic bone is commercialized and has no quantitative limitations and is inexpensive, but it has disadvantages of poor osseointegration due to immunological rejection and lack of osteoinduction ability. There are many restrictions on its use as its effectiveness has not been proven. Allogeneic bone has few limitations in its quantity and shape, as well as less histological rejection and good osseointegration. However, compared to autogenous bone, the osteoinduction ability is lower and the period required for bone union is long.[3)]

Therefore, the latest fracture healing methods are to apply patient-specific 3D printing, and it is the optimal fracture healing method that accurately prints and replaces implants that have been custom-made for bone tumor patients as well as skeletal defects caused by traffic accidents.

The patient specific 3D printing process is made through a series of processes of taking a patient's CT scan, performing symmetrical modeling of the defect compared to the normal part, and implanting the 3D printed output with a biocompatible material.[4)]

However, these recent application methods are not standardized and each hospital is selected differently according to its own internal process. So, in this study, to implement a standardized 3D printing process, we would like to apply the entire process of making a fracture model, manufacturing the customized 3D printing, and implanting it to animal experiments.[5)]

Ⅱ. MATERIALS and METHODS

Establishment of 3D printing process

The 3D printing process established an additional step by comparing the conventional surgical method and the 3D printing applied surgical method for fracture repair surgery (Figure.1). In general, when the standardized prosthetic implant is operated on an atypical fracture shape, the fracture-customized implant can be reproduced according to the patient's unique anatomy. A surgical reduction of tibia fractures grafted with 3D printing technology has established a surgical procedure through animal experiments. In the traditional fracture surgery method, the patient diagnoses the fracture through a medical image viewer and the patient, determines the treatment and surgery method, fixes the plate according to the fracture model, and evaluates the prognosis through postoperative radiographic analysis and patient behavior. The proposed 3D printing-applied fracture treatment process starts with radiographic image confirmation and fracture diagnosis, extract fractures and normal tibias as a 3D symmetric model from DCIOM files, and performs plate surgery after modeling a scaffold to replace fracture fragments. Finally, the process of confirming bone union by X-ray image shape analysis was constructed.[6)]

Fracture model

Among the previously established fracture models, the animal model for quantifying random tibia segments was 8-10 week old rats (male Sprague-Dawley, 357g-485g) (N = 8), and intraperitoneal injection of Rompun (xylazine) (20 mg/kg, Bayer) and Ketamine (80 mg/kg, Pfizer) were injected to perform general anesthesia. The left hind leg tibia of the rat was shaved, and the rat was fixed in the supine position. The devices used in the fracture model were added a steel frame, sliding plate, 500g weight, impactor and gravitational acceleration meter (Figure.2). The tibia fracture type was based on 3-point fracture, and the fracture was made by using a weight impactor to target the middle part located 20 mm below the proximal part of the tibia in 8-10 week old rats. Rats were randomized and divided into two groups (n = 8). Two groups of rats underwent posterior fractures 3 mm below the proximal left tibia. All rats were sourced from G-bio company and managed by Chosun University Biomedical Research Support Center. Chosun University Animal Care and Use Committee approved this research experiment and procedure (CIACUC2021-A0008).[7)]

The acquisition of Micro-Computed Tomography image

Rat tibia fracture scans were performed using a commercial micro-CT (Quantum GX; PerkineImer, Waltham, MA. U.S.A) at the Korea Basic Science Institute in Gwangju, Korea. The CON BEAM X-ray source was set at 90 kV and 80 mA with a field of view (FOV) of 72 mm (voxel size 144 μm, scan time 4 min, projection 512 pixels). 3D imaging was performed through a 3D viewer within the Quantum GX system. The resolution was set to 4.5 μm and fracture images were acquired in DICOM format (Figure.3).[6)]

Reconstruction

The extracted DICOM file is imported into medical image analysis commercial software (Mimics; Materialize NV, Leuven, Belgium). The DICOM image slice thickness of conventional plate surgery and 3D printing scaffold surgery was the same at 0.14399 mm, and 512 DICOM images each were automatically arranged in a line in coronal, sagittal, and transverse sections in the software. To visualize the DICOM data, the thickness was created by connecting the blank space between each image to successive singularities of the DICOM cross-section image in the stacked array and the overall shape was reconstructed (Figure.4). This process is automatically processed within the commercial software for medical image analysis.[8)]

The image isotropic conversion of 3D volume image

The two-dimensional plane data of the reconstructed CT was piled up, and the shape pre-visualization that maintained the original shape was implemented using volume rendering of the three-dimensional image. In isotropic conversion, the voxel size of the anisotropic CT data is normalized to have an isotropic volume, and interpolated data is added between each slice through sampling so that the entire interval size of the CT data images is the same.[15)] For image isotropic conversion, the automatic optimization process was implemented in real time in the medical image analysis commercial SW (Mimics innovation suite; Materialize, Leuven, Belgium) by applying the b-spline interpolation algorithm (Figure.5). For visualization of work progress, volume rendering is used and the method of storing data in units of voxels is applied. Whenever the observation area is changed through rotation and movement of the visualization view, the 3D volume rendering image is reconstructed by adjusting the resolution in real time.[9)]

Soft and hard tissue segmentation

A gray scale of a medical CT image is constructed using the Hounsfield unit (HU), which quantitatively expresses the intensity of transmitted X-rays. It represents values in 4096 steps (12 bits) from -1024 HU to 3071 HU in the range from black to white, and generally depends on the patient dose and resolution. In order to separate bone from muscle and adipose tissue from gray-scale images, a specific density value, which is a threshold, that forms the isodensity plane was extracted. By manually adjusting the minimum and maximum values of the slide bar for threshold setting, the threshold for muscle fat was setup from 2154 to 7000 and the threshold for bone from 2500 to 7500. Based on the threshold, the HU range included in the bone tissue was marked on each CT cross-sectional image by automatic and semi-automatic techniques, and the HU outside the range was treated as a muscle fat area excluding the bone and not marked.[10] In volume rendering, a real-time tibia model was extracted using the 3D Mask function to edit voxels in the bone threshold range (Figure.6).

STL format extraction of fracture bone

Through segmentation, the bone and non-bone regions were separated, and the border line of the cross-sectional area marked on the CT cross-sectional bone area was continuously connected. Then, a 3D surface model of an abnormal tibia is generated including the spine, pelvis, normal tibia, and tibia fragments generated by 3-point fracture. To ensure the consistency of tibial model extraction, a single anatomy expert performed a semi-automated tibial surface model separation process using commercial software for medical imaging analysis (Mimics innovation suite; Materialize, Leuven, Belgium). The rat lower body surface model data created for editing in CAD SW was extracted as a stereolithography (STL) file (Figure.7).

Symmetrical registration of tibia models

The surface shape model of the lower body of the rat imported into 3D CAD design SW (3ds max; Autodesk, San Rafael, U.S.A) was copied in a left-right symmetric form using mirror symmetry constraints based on the spine and pelvis. Two models were matched based on the singularity of the fractured tibia through movement and rotation of both femurs and tibias with the pelvis and spine removed (Figure.8).

Tibial fracture restoration

The tibia fracture type was classified according to the OTA/AO Classification of Tibia Diaphyseal Fractures, and tibia fracture repair was performed. After the fractured bone fragments were matched to the normal tibia model, the half-symmetrical model was removed. When the bone fragments connected to the tibia shaft are separated by shape, hollow holes appear on the joint surfaces of both models separated. 3D CAD design SW (3ds max; Autodesk, San Rafael, U.S.A) filled in the gap semi-automatically through interpolation. The filled bone fragments went through an additional model registration process to complete fracture repair (Figure.9).[11)]

Fracture merge

According to the tibia fracture type, selected bone fragments from the restored tibia were divided into tibia other than bone fragments, and several fragments were merged into one model for scaffold generation. The bone fragments need to be edited into a continuous surface, which erases the tangent surfaces of the areas to be joined. The rest of the tibia was created as a model to provide space for the merged bone fragments to be located. The crushed bone fragments are replaced by creating a shape replacement model instead of restoration (Figure.10).

Simulation for the 3D plate and scaffold position

The bone fragments merged for scaffold generation are subjected to positioning simulation in 3D CAD design SW (3ds max; Autodesk, San

Rafael, U.S.A) that combines the bone fragments and tibia. A 3D micro straight plate (OMF Micro System; TDM, Gwangju, Korea) with 5~8 holes created in advance in the virtual space of 3D CAD design SW was attached to the tibia fracture model. For the positioning of the plate fixing screw (Micro 1.5 system Bone Screw, TDM, Gwangju, Korea), the position of the plate was secured on the lateral side of the tibia, which is easily accessible from the tibia incision site. In actual surgery, depending on the fracture type classification, the surgical access position, plate size selection, and screw fixation position were limited in performing microscopic surgery in rats (Figure.11).

Scaffold model creation and Smoothing

After the corrected position of each model was confirmed through simulation, the surface model of the bone fragment and the pre-prepared lattice layer stacking model were merged. The three-dimensional scaffold created a layer in which 10 cylinders with a diameter of 0.5 mm and a length of 15 mm were arranged at 0.5 mm intervals. The printer head repeats array printing in which 10 layers to be stacked on top are rotated 90 degrees to the same size. Using the Boolean function of 3D CAD design SW (3ds max; Autodesk, San Rafael, U.S.A), only the intersection of the lattice model and the skeletal model was extracted to create a scaffold type bone fragment model. A smoothing function was applied to reduce noise on the surface of the lattice and tibia model (Figure.12).

Extract file format for 3D printing

For file processing to be sent to a 3D printer (CubiconSingle Plus; Cubicon, Gyeonggi-do, Korea), it was checked whether the 3D printer slicer SW (Cubicreator 3; Cubicon, Gyeonggi-do, Korea) supported a compatible STL file format. The scaffold bone model is set in a compact binary STL file format consisting of triangle vertices and surface normal vectors using the export tool of 3D CAD design SW (3ds max; Autodesk, San Rafael, U.S.A) and the file name is set. The file name was specified and extracted, then a 3D printer slicer SW checked STL file by importing. (Figure.13).[12)]

G-code and M-code generation

STL file was imported into 3D printer slicer SW (Cubicreator 3; Cubicon, Gyeonggi-do, Korea). The position in the output space of the scaffold bone model was equally centered around the 0,0,0 coordinates of the X, Y, and Z axes in the SW three-dimensional space. The area in contact with the 3D printer's heating bed was rearranged in consideration of the wide surface of the model and the optimal output direction of the print head. Then, the software sliced the 3D model in the STL format at regular intervals in each horizontal layer. Slicing divides the layers into layers along the Z-axis with a user-defined thickness, and converts them into machine-readable codes. The code content consists of the machine's travel path, including output profiles such as layer height, printing speed, and density. G-code sets the path coordinates to be optimally output by the 3D printer and occupies most of the code configuration. Codes starting with M execute commands to supply, cut off, and operate various hardware devices inside the 3D printer. Finally, the entire movement of the 3D printer head was confirmed through pre-visualization of the 3D model (Figure.14).[13)]

Surgical procedures

The fractured tibia was exposed through a 30 mm vertical skin incision along the anterior longitudinal axis. Medical experts removed the shredded bone fragments while minimizing damage to soft tissues such as periosteum and muscles for 3D printing scaffold surgery. Then, he set the screw positions of the micro straight plate (OMF Micro System; TDM, Gwangju, Korea) at the distal and proximal parts 3 mm away from the tibia fracture line, and placed the sterilized scaffold bone fragments between them. After securing the position, inject saline and pierce it with a 1.0 mm diameter drill bit (Mini electrical pen drill bit), and maintain a constant torque with a 1.2 mm diameter screw (Micro 1.5 system Bone Screw, TDM, Gwangju, Korea) vertically. The micro straight plate was pressed and fixed in the direction (Figure.16 a, b). After osseointegration, hemostasis and wounds were sutured with non-absorbable polypropylene sutures in the order of muscle and skin, and then disinfected. After recovery from anesthesia, rats were provided with a floor pad and food at 35° C for 5 days to enable movement, and were given animal antibiotics (0.2 mg/kg, Baytril; Elanco Animal Medicine, U.S.A) and veterinary analgesics (0.44 mg/kg, Analjin; Samyang anipharm, Korea) was administered, and the recovery status of the rats was continuously monitored until sacrifice.[14)]

Ⅲ. RESULTS

Scaffold Printing

The tibia-segment merging scaffold was made of a white PLA filament (PLA-i21; NatureWorks, MN, U.S.A) with a diameter of 1.75 mm and a 3D printer (CubiconSingle Plus; Cubicon, Gyeonggi-do, Korea) of the FFF type (Fused Filament Fabrication type) method.

The 3D printer melted the filament by setting the nozzle temperature to 210 ℃, and set the bed temperature to 65 ℃ to cool the laminated output. In addition, the 3D printer head extruded the scaffold layer to a height of 0.5 mm and stacked it in 4 layers. The printed tibia bone fragment scaffold is printed with two pseudo-tetrahedrons with a width of 6 mm, a length of 4 mm, and a height of 3 mm and a hexahedral model with a width of 10 mm, a length of 10 mm, and a height of 3.5 mm for small size printing calibration. During the output operation time of an average of 15 minutes, the printed scaffold shape and abnormality of the supporter are checked. After the printer head stops working, wait 10 minutes for the cooling time to separate the printer heating bed and the scaffold. Then, the printed scaffold is removed from the heating bed. After removing the support and finishing the surface post-treatment, the completed tibia scaffold was sterilized with alcohol (Figure.15).

Radiological analysis

X-RAY images showed the results of conventional surgery and 3D printing applied surgery for fractured tibia as follows.

After removing the fractured bone fragments, the conventional surgery in which the tibia was fixed with a plate conserving 4 mm defected space maintained the normal bone formation shape to fill the gap between the newly formed bone and the osteotomy in the X-ray obtained 4 weeks later. It is thought that the fracture site was stably fixed and continued bone regeneration was possible (Figure.16 a, Figure.17 a).

X-ray of rats with 3D-printed scaffold bone fragments were obtained 4 weeks after surgery and the shape was confirmed. In X-ray, the shape of osseointegration between the tibia fracture line and the scaffold maintained the segmented shape as immediately after fracture. It is thought that bone regeneration was difficult due to unstable fixation of the plate and screws surrounding the scaffold (Figure.16 b, Figure.17 b).

Ⅳ. DISCUSSION

This study carried out a series of procedures to apply the entire process of making a fracture model, manufacturing a customized 3D printed bone fragment, and implanting it in the defect site to 3D printing. In particular, it was intended to preserve the anatomical requirements of the segmented tibia, determine the appropriate design of the scaffold to merge and replace the bone fragments, and apply minimal surgical replacement using a 3D-printed scaffold.

This process that integrates fracture repair surgery and 3D printing application is expected to promote bone union and accelerate recovery time using 3D printing implants. In particular, it is possible to increase the possibility of 3D printing application by filling the scaffold with various osteogenic metabolism promoting materials in the osseointegration space.

Although it is necessary to obtain histological photographs and analysis data for histological analysis of bone union, this paper focused on experimenting with the 3D scaffold printing process for tibia fractures.

Various custom scaffolds are applicable for image-based 3D modeling, but the surgical process can be time-consuming due to differences in animal anatomy. For repeated confirmation studies, it may be better to select older or younger animals in future investigations to secure tibia recovery and consistency of scaffolds because long-term management problems and prognosis variability occur in elderly mice. Preoperative radiographic imaging may be appropriate to determine the appropriate scaffold design and print size for each animal prior to surgery. Since the size of the rat tibia trunk segment is very small, it is important to adjust the tibia diameter when modeling a small scaffold. In the case of high-resolution

(512×512 pixel) micro-CT image, it is possible to model the porous structure inside the bone marrow cavity as well as the perfect cortical bone shape. Animals with a larger tibia diameter than rats will facilitate analysis of the pore structure in the applied intramedullary cavity. Modeling of segmental bones on CT results in more segmental bones during actual surgery, and additional damage must be considered during the surgical process. In addition, in the case of choosing to use the tibia-segment bone merging alternative design for the scaffold, the change in the segment size should be determined according to the CT image and the segment situation directly seen during fracture surgery. Through a segmental bone fusion for bone marrow disintegration and repair, a single scaffold modeling is created and an indentation plate placed for support during tibia recovery is applied. Various segmental analysis data for optimal scaffold fit output in tibial interosseous segment fracture can be helpful in designing a segmental merge design model.

A limitation of this study is the lack of prognostic data through gait and continuous CT data confirmation after surgery recovery. For the quality of recovery after surgery, it will be useful to compare rat weight data at various time points, and gait analysis to determine the quality of movement will be useful. Also, the recovery function of rats was lowered due to the prolonged operation time, and there was a limitation in the analysis stage after surgery, and for this, the help of an experienced animal specialist would be necessary. In addition, it would be necessary to check various micro-CT imaging setting conditions, CT radiation dose, DICOM conversion, segmentation, reconstruction, intramedullary pore structure modeling, filament material selection, G-code generation and accuracy according to printing size, hardness of porous structure, post-treatment, material denaturation during disinfection and sterilization, additional tibia segment response during surgery, a scaffold fixation method on the plate, prognosis confirmation, gait and weight confirmation. Through various histological evaluations, it will be necessary to analyze the shape persistence and ossification progression in the tissue of the 3D printing scaffold. In the future, it is necessary to collect continuous prognostic data using micro-CT and X-RAY images and utilize them for comparative analysis. The expanded bone tissue material will be helpful in the application of 3D-printed scaffold pore surface bonding and the bonding of additive materials to promote bone formation.

V. CONCLUSION

In this study, 3D printing of tibia fracture scaffold bone fragments based on micro-CT images showed the entire process of implantation in the tibial fracture defect area, and a 3D printing-applied surgical process development model was proposed. In particular, the design of the combined scaffold model of the segmental tibia based on CT images allows the approach of surgical methods using 3D printed output and can reduce the risk of additional fracture. By designing and 3D printing immediately after a patient's CT scan, the parallel integration of real-time customized 3D printing and surgery will be possible.

REFERENCES

1. Choi, Eui-Sung & Shon, Hyun-Chul & Kim, Yong-Min & Kim, Dong-Soo & Park, Kyoung-Jin & Lim, Chae-Ouk & Lee, Hyung-Ki. (2016). Is the Incidence Rate of Hip Fractures still Increasing in Korea?: An Epidemiologic Study Based on National Health Insurance Database. Journal of the Korean Orthopaedic Association. 51. 447. 10.4055/jkoa.2016.51.6.447.
2. Lee KB. Distal tibia fracture: plate osteosynthesis. J Korean Fracture Soc. 2009; 22:306-313. doi:10.12671/jkfs.2009.22.4.306.
3. Roberts TT, Rosenbaum AJ. Bone grafts, bone substitutes and orthobiologics: the bridge between basic science and clinical advancements in fracture healing. Organogenesis. 2012;8(4):114-124. doi:10.4161/org.23306.
4. Seung-Won Choi; Park Kyung Soon; Yoon Taek Rim. Three-Dimensional Printing Technology in Orthopedic Surgery. Journal Of The Korean Orthopaedic Association. 2021; 56(2) 103-116. doi: 10.4055/jkoa.2021.56.2.103.
5. Salmi M. Additive Manufacturing Processes in Medical Applications. Materials (Basel). 2021;14(1):191. Published 2021 Jan 3. doi:10.3390/ma14010191.
6. Mitsouras, Dimitris and Liacouras, Peter and Imanzadeh, Amir and Giannopoulos, Andreas, RadioGraphics: Medical 3D Printing for the Radiologist.2015;35(7):1965-1988. doi: 10.1148/rg.2015140320.
7. Shi, E., Chen, G., Qin, B. et al. A novel rat model of tibial fracture for trauma researches: a combination of different types of fractures and soft tissue injuries. J Orthop Surg Res 14, 333 (2019). https://doi.org/10.1186/s13018-019-1386-4.
8. Lucas L. Geyer, U. Joseph Schoepf, Felix G. Meinel, John W. Nance, Jr,

Gorka Bastarrika, Jonathon A. Leipsic, Narinder S. Paul, Marco Rengo, Andrea Laghi, and Carlo N. De Cecco, Radiology: State of the Art: Iterative CT Reconstruction Techniques.2015;276:2: 339-357. doi:10.1148/radiol.2015132766.

9. Dimitrios Piretzidis, Michael G. Sideris, Stable recurrent calculation of isotropic Gaussian filter coefficients, Computers & Geosciences Volume 133, 2019,104303,doi: 10.1016/j.cageo.2019.07.007.
10. M.H. Lev, R.G. Gonzalez, CT Angiography and CT Perfusion Imaging, Academic Press, 2002, 427-484,ISBN 9780126930191, doi.org/10.1016/B978-012693019-1/50019-8.
11. Rudge, Will & Newman, Kevin & Trompeter, Alex. (2014). Fractures of the tibial shaft in adults. Orthopaedics and Trauma. 28. 10.1016/j.mporth.2014.03.002.
12. Kai, C.C., Jacob, G.G.K. & Mei, T. Interface between CAD and Rapid Prototyping systems. Part 2: LMI — An improved interface. Int J Adv Manuf Technol 13, 571-576 (1997). https://doi.org/10.1007/BF01176301.
13. ISO 6983-1:2009, Automation systems and integration — Numerical control of machines — Program format and definitions of address words — Part 1: Data format for positioning, line motion and contouring control systems.
14. Kang HP, Ihn H, Robertson DM, Chen X, Sugiyama O, Tang A, Hollis R, Skorka T, Longjohn D, Oakes D, Shah R, Kohn D, Jakus AE, Lieberman JR. Regional gene therapy for bone healing using a 3D printed scaffold in a rat femoral defect model. J Biomed Mater Res A. 2021 Nov;109(11):2346-2356. doi: 10.1002/jbm.a.37217. Epub 2021 May 21. PMID: 34018305.

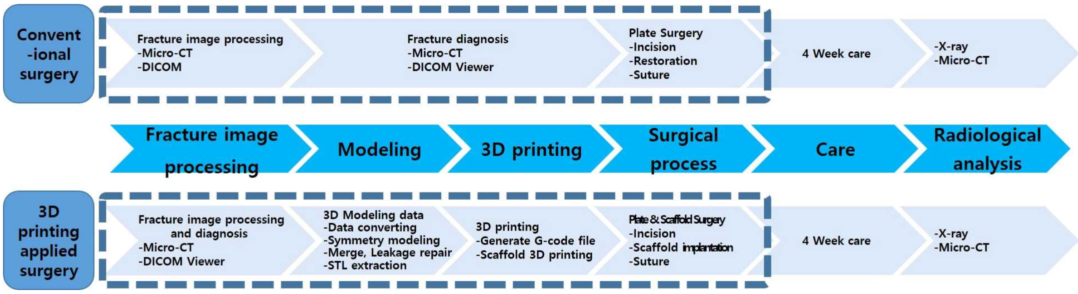

Figure 1. The 3D printing application process to rat tibia fracture model

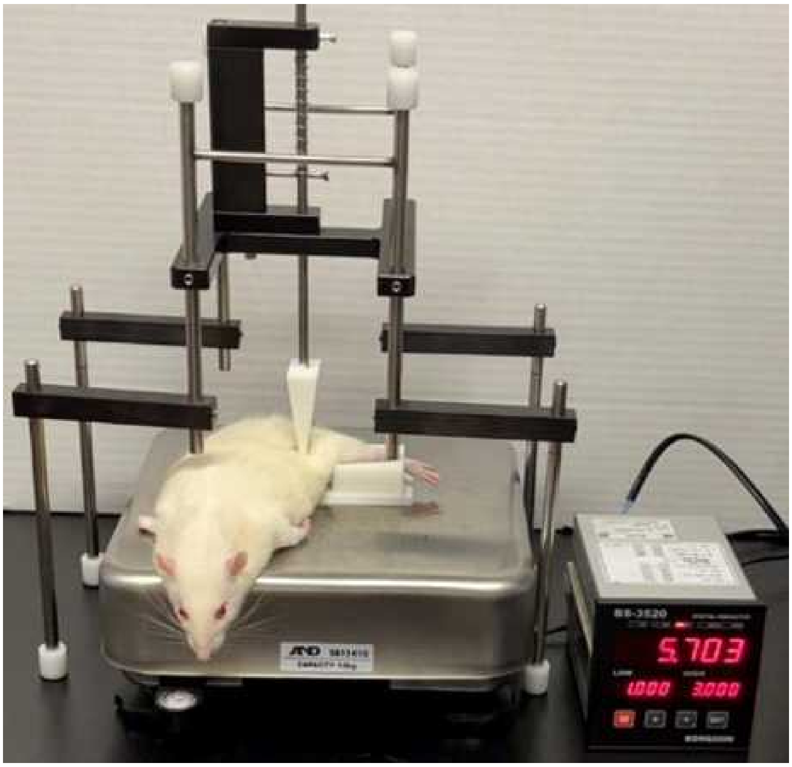

Figure 2. The apparatus for rat tibia fracture model

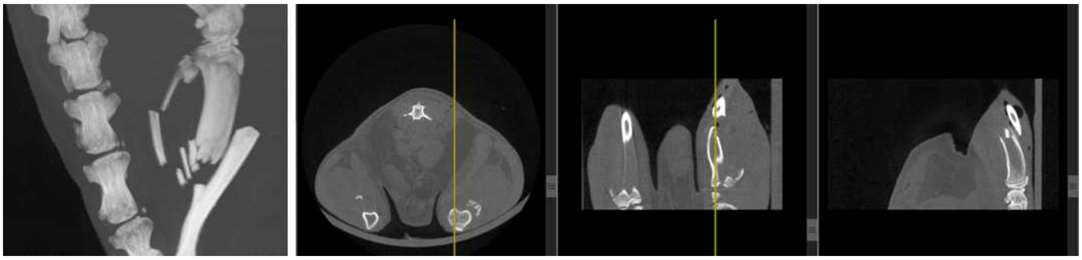

Figure 3. The Acquisition of rat tibia fracture images acquired through X-ray and micro-CT

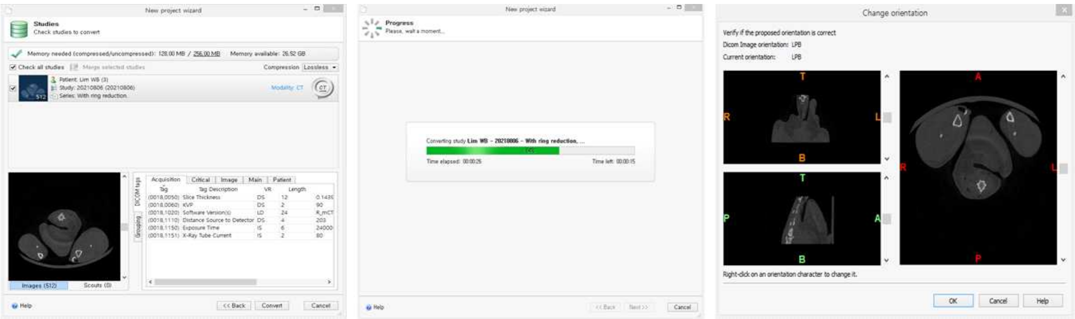

Figure 4. Based on the information of the DICOM file read from commercial software and the slice interval value, this is the micro-CT cross-sectional image array conversion process and viewpoint direction setting step

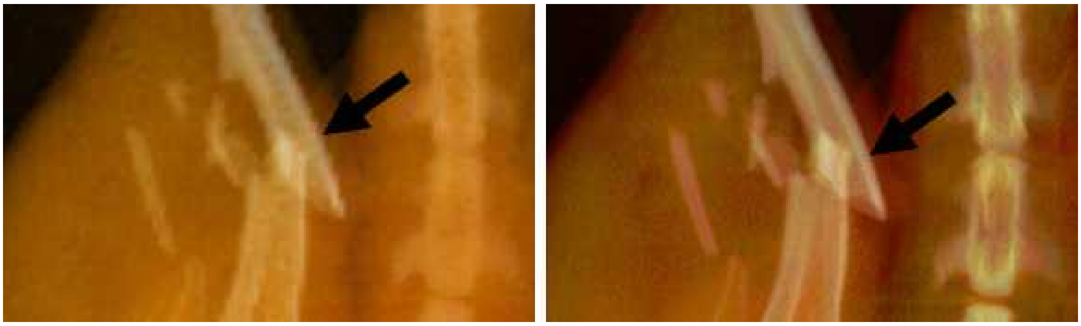

Figure 5. A Comparison of differences before and after the image isotropic conversion confirmed through volume renderer. Anisotropic voxel that causes aliasing is converted into isotropic voxel to generate high-resolution voxel images

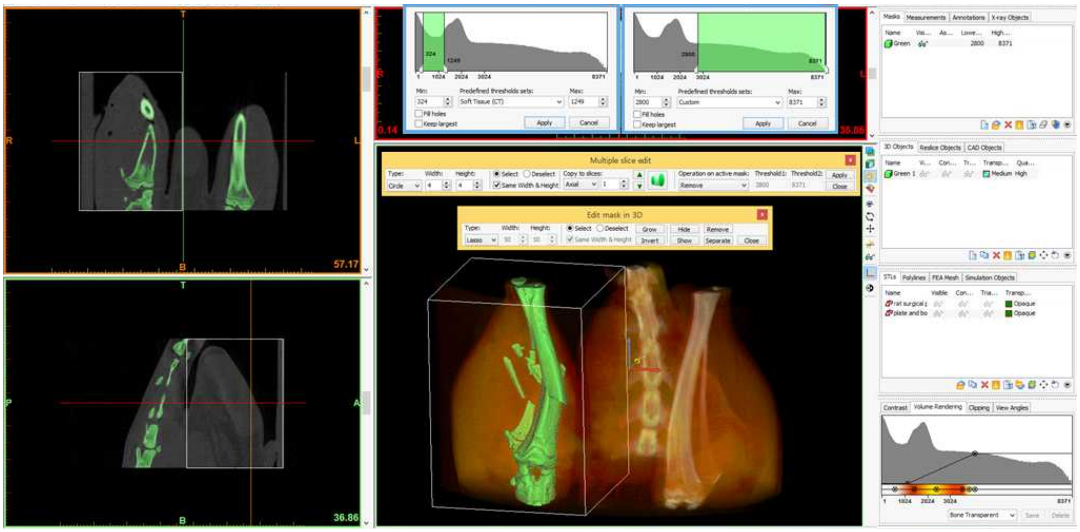

Figure 6. The separation of bone and soft tissue (muscle, fat) in the gray scale area of the radiographic image. Threshold and soft tissue threshold settings for bone extraction and volume visualization segmentation workflow

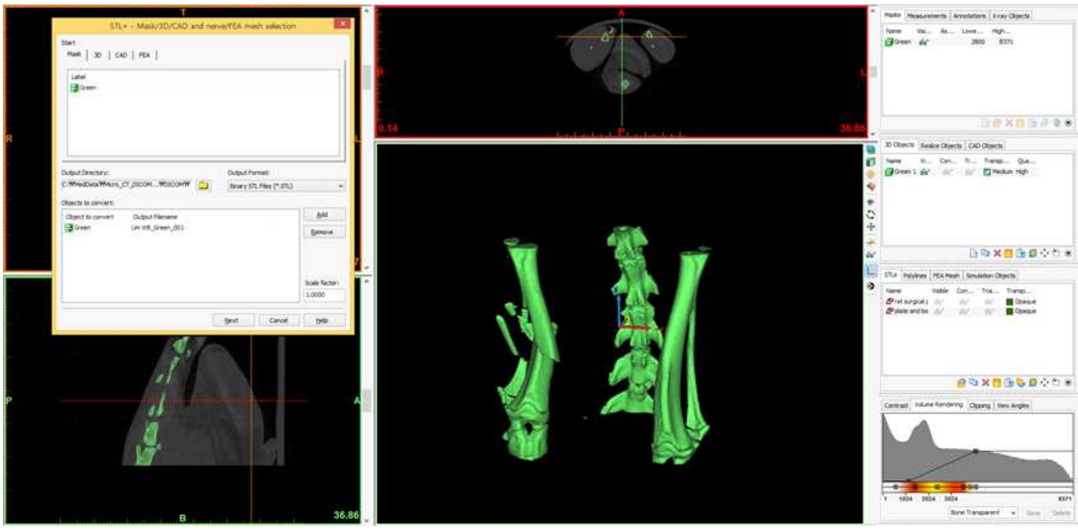

Figure 7. Steps to extract the bone 3D model separated by segmentation as a STL file

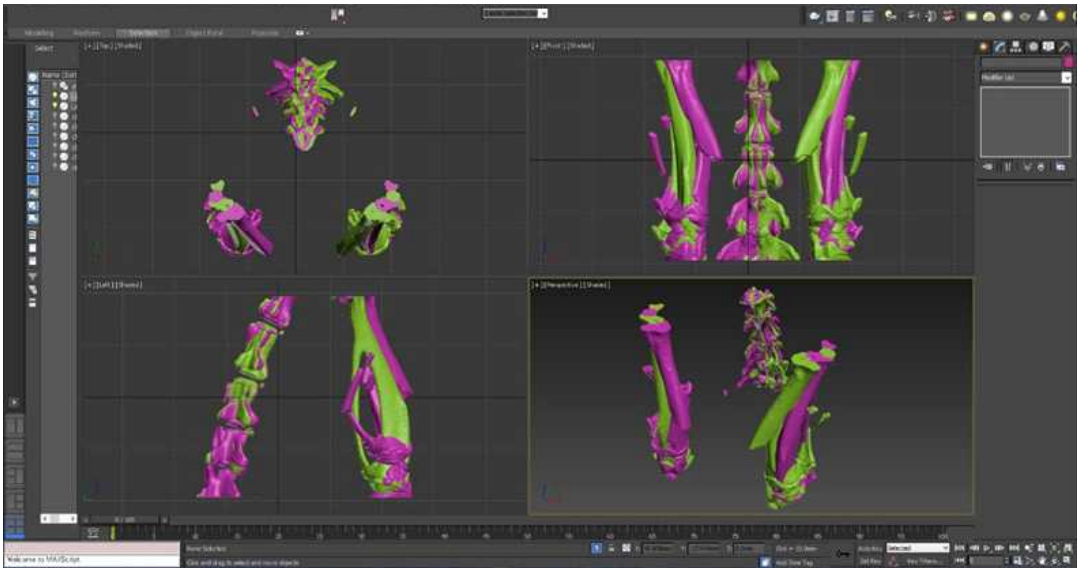

Figure 8. Shape alignment after mirroring of left and right tibia bone model

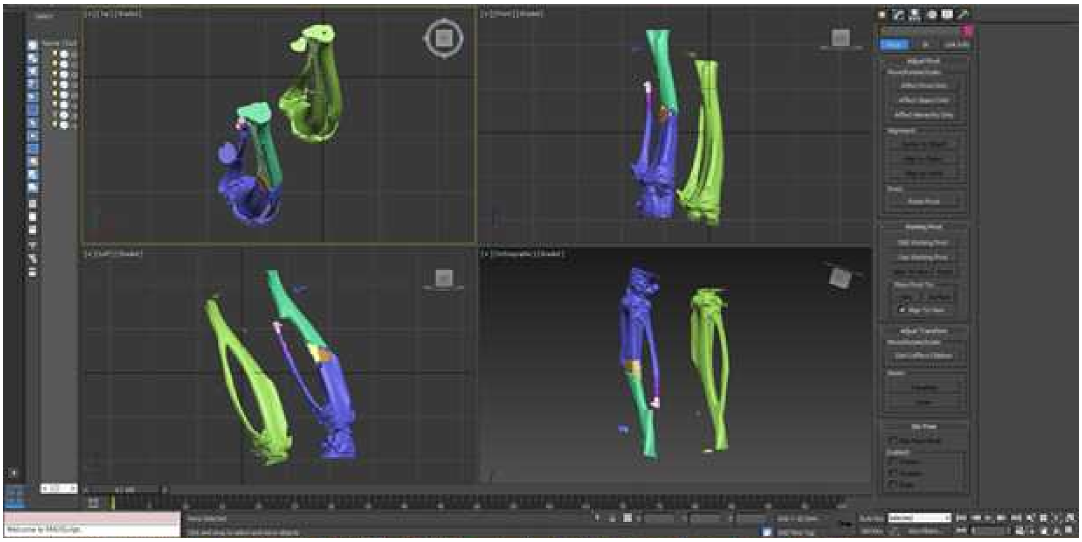

Figure 9. The tibial fracture repair process through 3D bone fragment model reconstruction

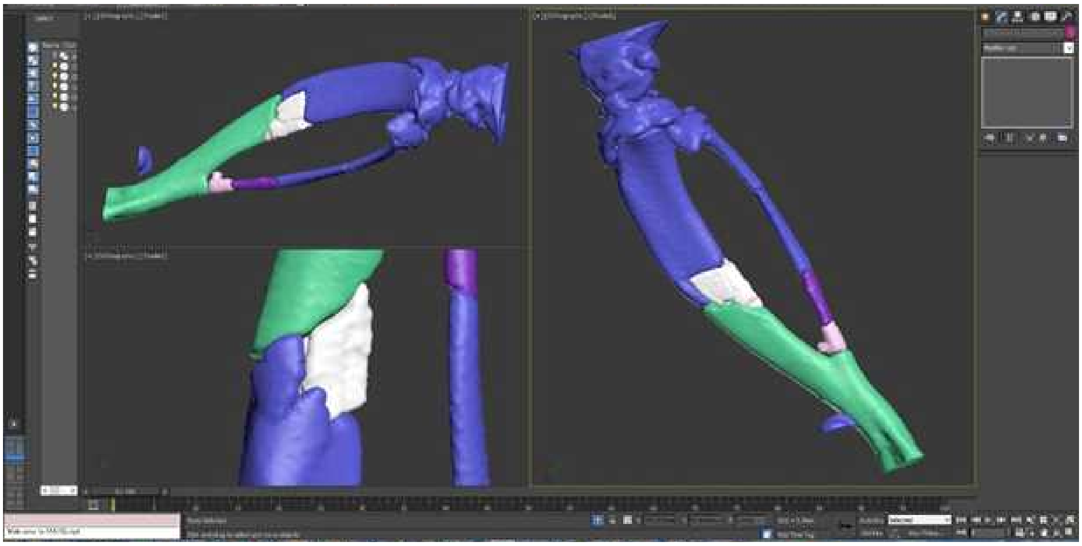

Figure 10. 3D bone fragments are merged into a single bone fragment and generated as a replacement model of fractured fragments

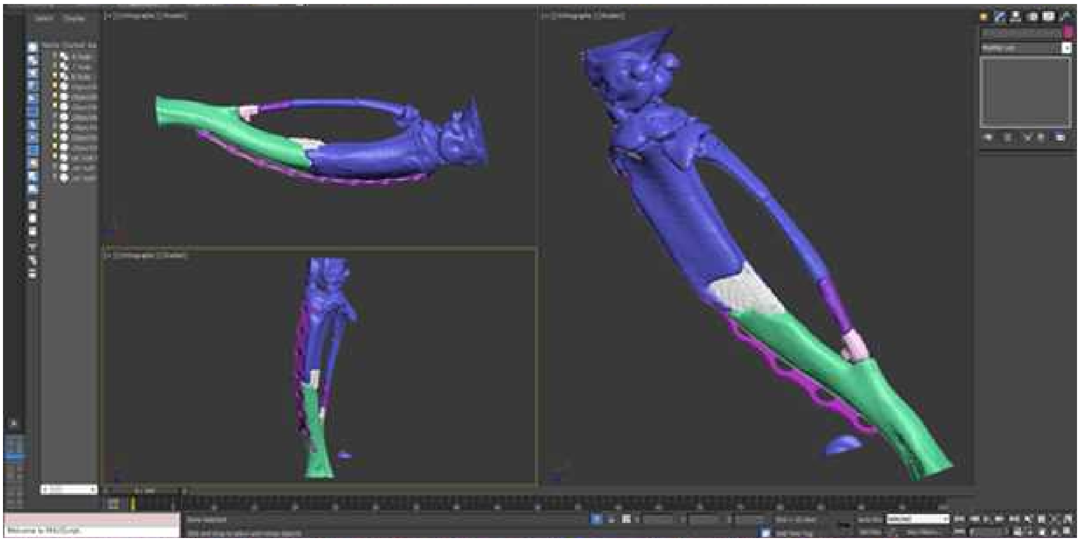

Figure 11. Simulation for selection of an open surgical site and positioning of plate screws

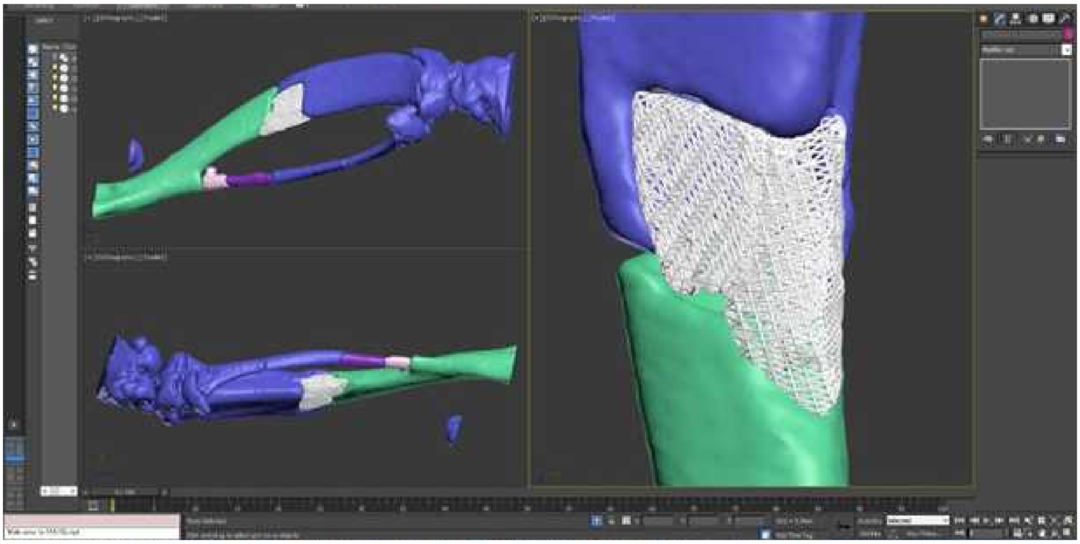

Figure 12. Applying smoothing function for lattice modeling and surface noise reduction in 3D CAD design SW

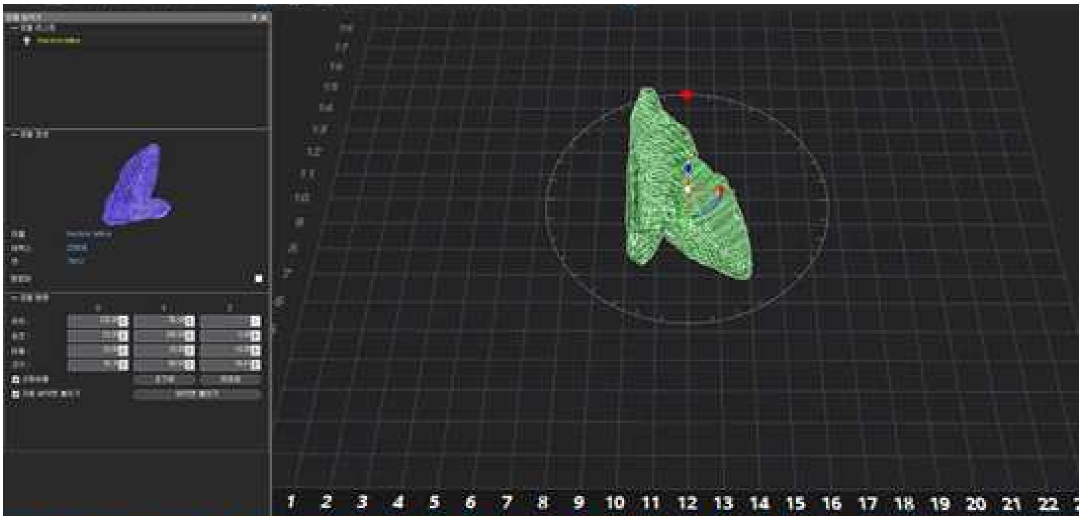

Figure 13. The 3D Printer Slicer SW imports and checks the extracted scaffold bone model in STL format

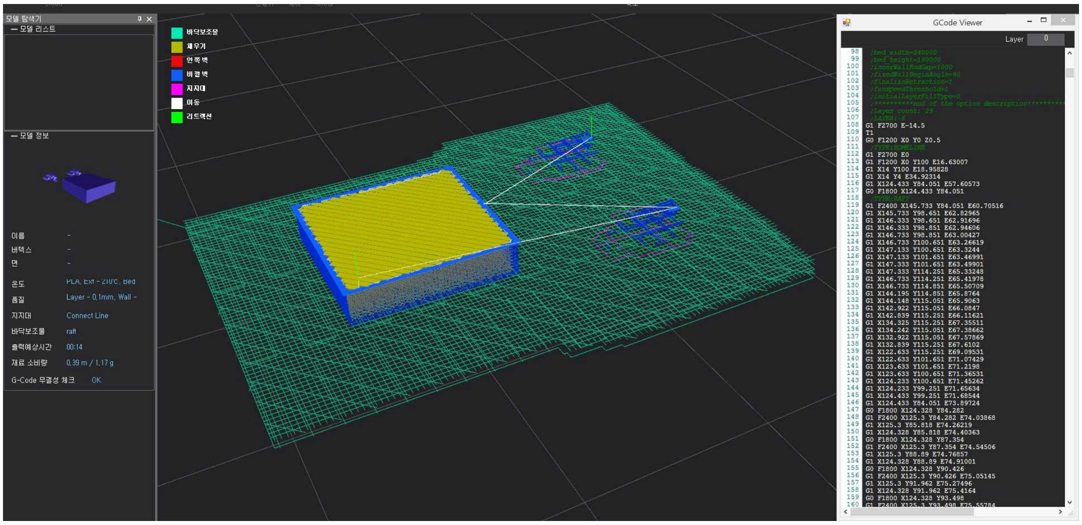

Figure 14. The G-code composition and pre-visualization process of 3D printing movement

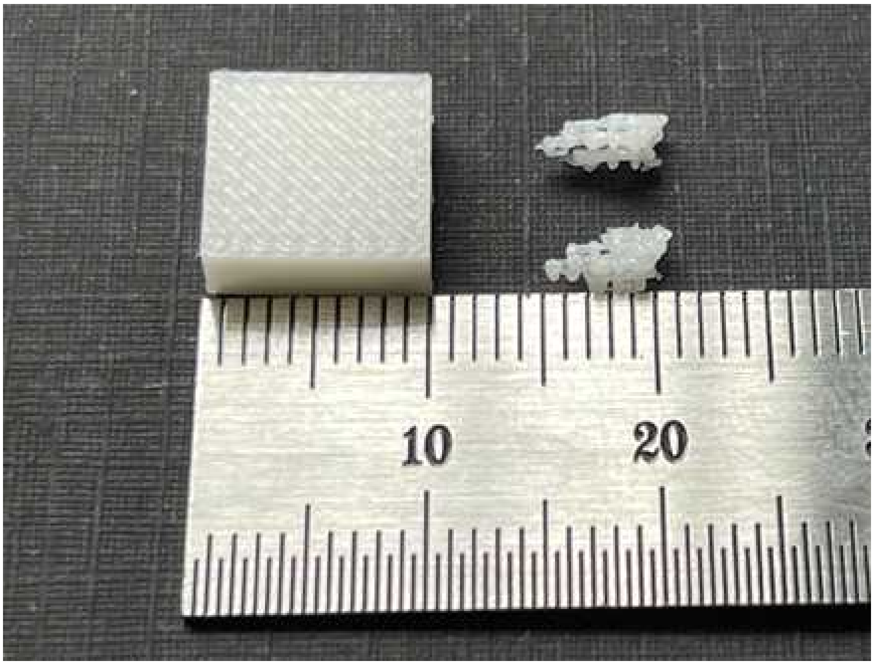

Figure 15. The size of the calibrating hexahedron for fine 3D printing and 3D printed two scaffold bone fragments

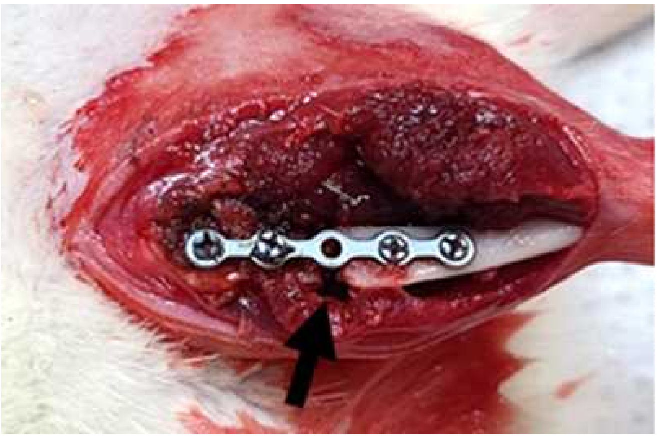

(a)

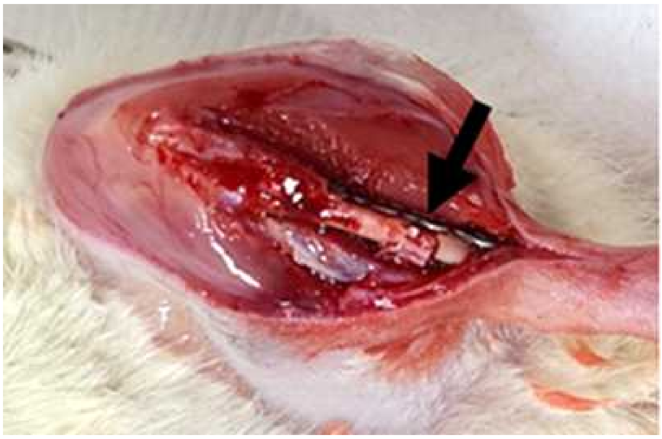

(b)

Figure 16. A view of the rat tibia fracture immediately after conventional method surgery (a) and a view immediately after the 3D printed scaffold surgery (b)

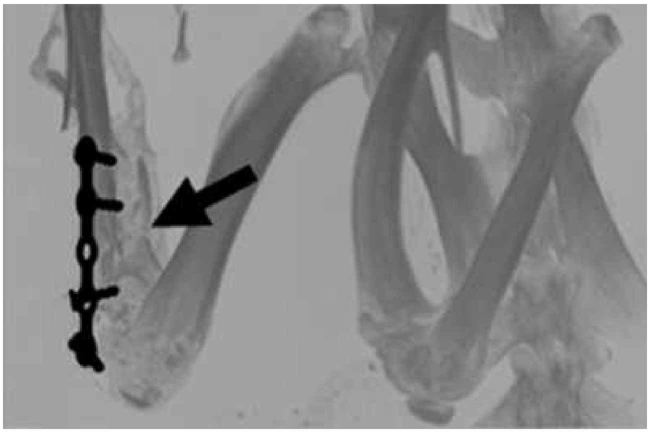

(a)

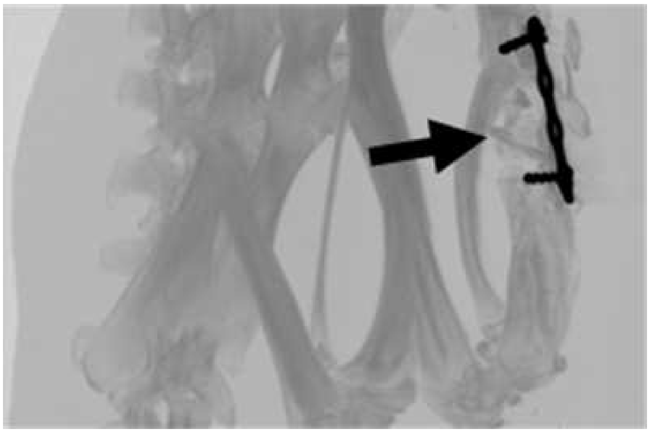

(b)

Figure 17. X-ray comparison of conventional surgical method (a) and 3D printing application method (b) for tibia fracture after 4 weeks